Identification the Roles of Ferroptosis-Related Gene Signatures in Patients with Esophageal Adenocarcinoma

Lei Zhu
Tongji University School of Medicine
Fugui Yang
Tongji University School of Medicine
Lingwei Wang
Tongji University School of Medicine
Lin Dong
Tongji University Affilliated East Hospital: Shanghai East Hospital
Zhiyuan Huang
Tongji University School of Medicine
Guangxue Wang
Tongji University Affilliated East Hospital: Shanghai East Hospital
Guohan Chen
Tongji University Affilliated East Hospital: Shanghai East Hospital
Qinchuan Li (2857039377@qq.com)
Tongji University School of Medicine https://orcid.org/0000-0001-5133-7840

Primary research

Keywords: esophageal adenocarcinoma, ferroptosis, bioinformatics analysis, TCGA

Posted Date: November 17th, 2020

DOI: https://doi.org/10.21203/rs.3.rs-105346/v1

Version of Record: A version of this preprint was published on February 18th, 2021. See the published version at https://doi.org/10.1186/s12935-021-01821-2.

Abstract

Background Ferroptosis is a recently recognized non-apoptotic cell death that is distinct from the apoptosis, necroptosis and pyroptosis. Considerable studies have demonstrated ferroptosis is involved in the biological process of various cancers. However, the role of ferroptosis in esophageal adenocarcinoma (EAC) remains unclear. The aim of this study was to explore the ferroptosis-related genes (FRG) expression profiles and their prognostic values in EAC.

Methods The FRG data and clinical information were downloaded from The Cancer Genome Atlas (TCGA) database. Univariate and multivariate cox regressions were used to identify the prognostic FRG, and the predictive ROC model was established using the independent risk factors. GO and KEGG enrichment analyses were performed to investigate the bioinformatics functions of significantly different genes (SDG) of ferroptosis. Additionally, the correlations of ferroptosis and immune cells were assessed through the single-sample gene set enrichment analysis (ssGSEA). Finally, significantly different genes were verified in our clinical EAC specimens and normal esophageal mucosal tissues.

Results: Twenty-eight significantly different FRG were screened from 78 EAC and 9 normal tissues. GO and KEGG enrichments showed these SDG were mainly related to the iron-related pathways and metabolisms of ferroptosis. Gene network demonstrated the TP53, G6PD, NFE2L2 and PTGS2 were the hub genes in the biology of ferroptosis. Cox regression analyses demonstrated four FRG (CARS1, GCLM, GLS2 and EMC2) had prognostic values for overall survival (OS) (all $P<0.001$). ROC curves showed better efficacy to predict survival using the risk score (AUC=0.744). Immune cell enrichment analysis demonstrated that the types of immune cells and their expression levels in the high-risk group were significant different with those in the low-risk group (all $P<0.05$). The experimental results confirmed the ALOX5, NOX1 were upregulated and the MT1G was downregulated in the EAC tissues compared with the normal esophageal mucosal tissues (all $P<0.05$).

Conclusions: We identified differently expressed ferroptosis-related genes that may involve in the process in EAC. These genes have significant values in predicting the patients' OS and targeting ferroptosis may be an alternative for therapy. Further studies are necessary to verify these results of our study.

Background

Esophageal cancer is the eighth most common malignancy in the world, which accounts for approximately 570000 new cases and 50000 deaths per year worldwide [1]. Esophageal adenocarcinoma (EAC) is one of the main pathological types, characterized by high incidence and poor prognosis [2]. It's estimated that the proportion of patients with EAC nearly doubled, from 35–61% over the past 30 years in the western countries, with a global incidence rate of 0.7 per 100,000 person-years [3–4]. Despite the tremendous progress have been made in therapy, including the esophagectomy, radiation, chemotherapy and molecular targeted drugs, the 5-year survival rate still remains less 20% [3]. Therefore, an optimal management aiding in the early detection and therapeutic improvements is imperative. The latest studies

have showed ferroptosis, a non-apoptotic programmed cell death, has emerged to play an important role in tumor biology and may open up new opportunities for EAC [5–6].

Ferroptosis, firstly proposed by Stockwell BR lab in 2012, is a necrotic cell death modality that is morphologically, biochemically and genetically distinct from apoptosis, necrosis and autophagy [7]. This process is marked by the accumulation of reactive oxygen species (ROS) via an iron-dependent mechanism [7]. An initial characterization of the mechanism triggering ferroptosis is the cysteine depletion, which leads to the exhaustion of glutathione (GSH) in the intracellular [7]. Hence fore, it's conceivable a complex interplay that regulates the different cancer cell susceptibilities to ferroptosis should be a fruitful area in cancer research. A large amount studies have confirmed many genes are involved in the initiation and execution of ferroptosis in cancers [8–10]. These discoveries have shed light on the tumor ferroptotic plasticity and provided insights into how ferroptosis is associated with the persistence, dedifferentiation and expansion of cancer cells. In addition, evidence from several researches have demonstrated the ferroptotic cells could interact with NK cells, CD8 + T cells and other immune cells by releasing some chemotaxis, thus modulating the anticancer immunity [11–13]. However, it's undeniable that much less clear about how the ferroptosis is elaborately regulated and it is far from applying the ferroptosis to cancer therapy.

A better understanding of ferroptosis is critical for immune surveillance and therapeutic management, as well as paving ways for further explorations. To our best known, there is scarce study exploring the link between the ferroptosis and EAC, and their relationships with survival in EAC patients have never been studied. In this study, we aim to investigate the ferroptosis-related genes (FRG) expression profiles and their values in the prognosis in EAC through the bioinformatics analysis. The results were verified in our clinical specimens using the clinical specimens.

Methods

Acquisition of gene expression and clinical data

Both gene expressions of transcriptome profiles and clinical data of EAC patients were downloaded from The Cancer Genome Atlas (TCGA) website at https://portal.gdc.cancer.gov/. The raw data of gene expression was normalized using the "limma" R packages in R software (version 4.0.2). The 60 FRG were retrieved from previous published literatures and the FRG were available in the Supplementary Table S1 [14–17].

Identification of significantly different genes and prognostic factors

The significantly different genes (SDG) were identified using the "limma" R packages with the Wilcoxon test. The cut-off values were determined according to the parameters, $P < 0.05$ and false discovery rate (FDR) < 0.05.

Univariate and multivariate cox regression was used to evaluate the relationships between the SDG among the FRG and the patients' overall survival (OS). Patients were divided into high-risk and low-risk groups according to the risk scores. The risk score was calculated by the following formula: risk score = $\sum_{n=1}^{j} Coefj * Xj$, with Coef j representing the coefficient and Xj representing the relative expression levels of each SDG standardized by z-score.

Interaction network of SDG and enrichment analysis

An interaction network of SDG was performed at the online STRING website (http://string-db.org/cgi/input.pl). Then, we also explored their correlations using the R software.

Next, the functional enrichment analysis of Gene Ontology (GO), including the biological process, cellular component, and molecular function was performed by R software. The Kyoto Encyclopedia of Genes and Genomes (KEGG) analysis was also done using the same tool.

Development of ROC curves

Then, we combined the prognostic FRG with clinical information using the univariate cox regression. Significant prognostic factors ($P < 0.05$) were enrolled into multivariate cox regression to identify the independent prognostic risk factors. The Receiver Operating Characteristic (ROC) analysis was used to examine the sensitivity and specificity of survival prediction using the independent risk factors. The area under curve (AUC) of the ROC ranges from 0.5 to 1, with near 1 indicating perfect predictive ability and 0.5 indicating without predictive ability.

Immune cell and their functions

At last, we evaluated the infiltrating score of 16 immune cells and the activity of 13 immune-related pathways using the prognostic FRG with the single-sample gene set enrichment analysis (ssGSEA) in the "gsva" R package [18]. The annotated gene set file is provided in Supplementary Table S2.

Experimental validation

To verify SDGs expression profiles in EAC and normal tissues, we conducted the experimental validation in 15 EAC patients' specimens who received esophagectomy from 2019 January to 2020 June in Shanghai East Hospital, Tongji University School of Medicine. Ten normal esophageal mucosal tissues were used as control. This study was approved by the Internal Review Board of Shanghai East Hospital, Tongji University School of Medicine.

Total RNA from EAC specimens and normal tissues was purified using RNAiso plus (Takara, Dalian, China). Complementary DNA (cDNA) was synthesized from 1 μg of total RNA using a PrimeScript® RT reagent Kit with gDNA (genomic DNA) Eraser (Takara). TB Green® Premix Ex Taq® II kit (Takara) was used to detect the indicated RNA levels on the QuantStudio Real-Time polymerase chain reaction (PCR) System (Applied Biosystems, USA) or the CFX96 Real-Time System (Bio-Rad, USA). The relative expression levels of the candidate ARGs were normalized to endogenous GAPDH (glyceraldehyde-3-

phosphate dehydrogenase). The primers synthesized and by GENEWIZ company, Suzhou, China. The primers are listed in Supplementary Table S3.

Statistical analysis

Student's t-test was used to compare gene expression differences between tumor tissues and normal tissues. Univariate and multivariate cox regression analysis were used to evaluate the correlation between the factors and patients OS. Log-rank test was used to compare the survival differences between high and low-risk groups. Kaplan-Meier curve was implemented to visualize the survival. Mann-Whitney test with P values adjusted by the BH method was used to compare the ssGSEA scores of immune cells or pathways between the high-risk and low-risk groups. All the statistic were analyses were done using the R software (version 4.0.2). P value < 0.05 was set as statistically significant for all the analyses.

Results

Identification of SDG and patients' clinical data

A total of 9 normal samples and 78 EAC samples with gene expression profiles and clinical information were retrieved from the TCGA datasets. After analysis, there were 28 significantly different genes between normal and EAC samples. Among these FRG, four FRG (AKR1C1, AKR1C2, MT1G and NFE2L2) were down-regulated in EAC tissues compared with normal tissue, other 24 genes were up-regulated (Table 1). The heatmap and deviation plots were shown in Fig. 1a-b.

Figure 1 Identification of SDG in normal and EAC tissues. (a) heatmap of SDG. Green represented down-regulation and red represented up-regulation of genes. (b) deviation plot of SDG. Yellow bars represented 4 down-regulated genes; blue bars represented 24 up-regulated genes. N: normal, T: tumor (EAC).

Functional enrichment analysis of SDG

To elucidate the biological functions and pathways of SDG in ferroptosis, the 28 genes were used to performed GO and KEGG analysis. The GO results showed that SDG were enriched in iron-related pathways, such as metabolic and oxidative process. As expected, the KEGG analysis also obviously showed the SDG were enriched in ferroptosis, including the GSH metabolism, oxidative reaction and biosynthesis (Fig. 2a-d).

Figure 2 Representative results of GO (a, c) and KEGG (b, d). bubble plot of GO (a) and KEGG (b) analyses. Results of GO (c) and KEGG (d) in the form of gene ID. The larger bubble indicates the more obvious enrichment.

Interactions and correlations of SDG

We explored the SDG interactions in the STRING online website, the gene network demonstrated the TP53, G6PD, NFE2L2 and PTGS2 were the hub genes (Fig. 3a). The correlations between these SDG are

Figure 3 Gene interactions and correlations plots of SDG. (a)The gene network downloaded from the STRING database indicated the interactions among the SDG. (b)The correlation network of genes. Red line represents the positive correlation, while the blue line represents the negative correlation.

Prognostic FRG and independent risk factors

Nearly half of the FRG (46.67%, 28/60) were differently expressed in the normal and EAC tissues. By performing the univariate cox regression analysis in the 78 EAC patients, we identified four FRG (CARS1, GCLM, GLS2 and EMC2) were significantly associated with OS (all $P < 0.001$) (Fig. 4a). Subsequent multivariate cox regression analysis indicated that only one ferroptotic gene (GLS2) were independent prognostic risk factor (HR = 6.328, P = 0.004) (Fig. 4b).

According the median of the risk score (risk score formula = 0.781 * expression level of CARS1 + 0.474 * expression level of GCLM + 1.845 * expression level of GLS2 + 0.717 * expression level of EMC2), patients were stratified into high and low-risk groups. Then, we explored the clinical information values in the patients' OS combining with the FRG. In the results of univariate cox analysis, we found that tumor stage and risk score were significantly associated with OS (all $P < 0.05$) (Fig. 4c). And the multivariate cox regression showed the tumor stage and risk score were independent risk factors in EAC patients' OS (HR = 6.755, HR = 1.328, all $P < 0.001$ respectively) (Fig. 4d).

Figure 4 Results of the univariate and multivariate cox analysis of the OS in EAC patients. FRG prognostic values in the univariate (a) and multivariate cox analysis (b). Risk factors analysis of OS in the univariate (c) and multivariate cox regression (d). HR: hazard ratio.

Prognostic hazard curves in high and low-risk patients

Seventy-eight EAC patients were divided into high-risk group (n = 39) and low-risk patients (n = 39) according to the median of the risk score. The Kaplan-Meier curve showed patients with high-risk score had a significant higher death probability than those with low-risk (median time = 0.657 years vs. 1.192 years, p = 0.0075, Fig. 5a). As the risk score increased, the patients' death risk increased, and the survival time decreased (Fig. 5b, 5d). The risk heatmap clearly showed EMC2 was up-regulated in high-risk group compared with the low-risk group, implying it was a tumor-promoting role (Fig. 5c).

Figure 5 Kaplan-Meier curve and prognostic hazard curves. Kaplan-Meier survival curve (a). Risk score curve plot (b). The dotted line indicated the individual inflection point of the risk score curve, by which the patients were categorized into low-risk (green) and high-risk (red) groups. Risk score heatmap (c). The colors from green to red indicated the expression level from low to high. Risk score scatter plot of high-risk and low-risk (d). Red dots represented the dead patients and green represented the alive. With the increase of risk score, more patients died.

Construction predictive models

In order to provide an applicable method to predict the EAC patients' OS, we established the ROC curve using the independent risk factors (risk score) from the multivariate cox regression.

In addition, we also assessed the feasibility using the area under curve (AUC) value. The results showed the risk score had better predictive ability (AUC = 0.744) (Fig. 6).

Figure 6 ROC curve of risk score. The AUC ranges from 0.5 to 1.0, with near 1.0 indicating perfect predictive ability.

Immune cell enrichment analysis

To further explore the relationships between the risk score and immune cell and functions, we quantified the enrichment scores of 16 immune cell subpopulations and their related functions with the ssGSEA R package. The results showed the types of immune cells (such as DCs, iDCs, mast cells, Th2 cells, TIL cell, Treg cells, B cells, CD8 + T cells, pDCs, T helper cells, Th1 and Tfh cells) in the high-risk group were significant different with those in the low-risk group (Fig. 7a). Moreover, the scores of the immune functions, such as the type I IFN response, type II IFN response, T cell co-inhibition, APC inhibition and check-point were significantly higher in low-risk group, implying their immunological functions associated with ferroptosis were more active in the low-risk group (Fig. 7b).

Figure 7 Comparison of the ssGSEA scores between the high-risk and low-risk groups. The scores of 16 immune cells (a) and 13 immune-related functions (b) are displayed in boxplots. DC: dendritic cell; TIL: tumor infiltrating lymphocyte; CCR: cytokine-cytokine receptor; APC: antigen presenting cells. Adjusted P values were showed as: ns, not significant; *, P < 0.05; **, P < 0.01; ***, P < 0.001.

Clinical experimental validation

We performed the validation in clinical specimens following the steps described above. We verified the five most significantly different genes from FRG according the logFC values (NOX1, MT1G, PTGS2, ALOX5, TFRC). By comparison, the PCR results showed MT1G were down-regulated and the ALOX5 and NOX1 were significantly up-regulated in the EAC tissues. There were no significant differences in the expression of PTGS2 and TFRC between the normal and EAC specimens. The details of the five genes were visualized in Fig. 8a-e.

Figure 8 The relative expression levels of the five genes in normal and EAC tissues. The ALOX5 (a), NOX1 (c) were up-regulated significantly and MT1G (b) were down-regulated in the EAC tissues. No significant differences were observed in the PTGS2 (d) and TFRC (e). *: P < 0.05; **: P < 0.01, ns: not significant.

Discussion

Cell death is a vital necessity for maintaining homeostasis, development and the prevention of excessively proliferative malignancy, such as cancer. To sustain the infinite self-renewal capacity, cancer cells exhibit the overwhelming demands for supply, including the energy metabolism, (anti)oxidant modification and iron intake [14]. The iron-dependent mechanism makes cancer cell more susceptible to iron-catalyzed necrosis, namely ferroptosis [7]. The proposal of ferroptosis has challenged the previous dogma that almost cell deaths were subject to the caspase-dependent apoptosis. Ferroptosis has

highlighted the significance of iron metabolism and created a new promising area combining with caner management. This unique type of death has attracted considerable studies exploring the ferroptotic potential mechanisms and pathways in various cancers [19–21]. However, the specific role of ferroptosis in EAC is unclear. In the current study, we systematically investigated the ferroptosis-related genes expression profiles in EAC. We found that almost half of genes (46.67%, 28/60) were expressed obviously different between the EAC and normal tissues. Functional enrichment analyses results showed these genes were mainly associated with iron-related pathways, such as metabolic and oxidative process. Survival analysis showed four genes (CARS1, GCLM, GLS2 and EMC2) had prognostic values. In addition, the immune cell enrichment analysis revealed the ferroptosis had a close connection with tumor immunity. These findings strongly implied the great potential roles of ferroptosis in EAC.

The essence of ferroptosis is a metabolic necrosis triggered by an iron-catalyzed excessive peroxidation of polyunsaturated fatty acids (PUFAs) [7]. Non-enzymatic lipid peroxidation or auto-oxidation of lipids is indispensable for the initiation of the PUFAs oxidation [22]. Beyond these, enzymatic lipid peroxidation is another chain reaction to catalyze the PUFAs mediated by lipoxygenase (LOX) family [15, 23]. The toxic consequence of continuous oxidation is the loss of the membrane integrity, leading to the occurrence of ferroptosis ultimately. Consistent with our results, functional enrichment analysis of this study demonstrated these different expressed FRG were mainly associated with the oxidative and iron-related reactions. In addition, the GO and KEGG results also showed there was a close link with GSH metabolism and biosynthesis. GSH, an anti-oxidant, could regulate the sensitivity and resistance of ferroptosis by serving as a cofactor for GPX4 (a member of enzymes) to reduce the lipid hydroperoxides [24–25]. GSH could be able to reduce the accumulation of phospholipid hydroperoxides and be responsible for the detoxification. Direct or indirect inhibition of GSH can induce the initiation of ferroptosis [8]. Therefore, it's conceivable that, anti-cancer therapy that targeting GPX4 and /or GSH may bring satisfactory effect.

The survival analysis and prognostic ROC models were developed based on four genes (CARS1, GCLM, GLS2 and EMC2) in this study. The FRG can be roughly classified into four categories according to their functions in ferroptosis: iron metabolism, lipid metabolism, (anti)oxidant metabolism (CARS1, GCLM) and energy metabolism (GLS2, EMC2) [14–15]. Among these, GLS2 (Glutaminase) is an independent risk factor for OS in patients with EAC in our study. The human GLS2 gene is located in chromosome 12, consisting of 18 kb and 18 exons [26]. The GLS2 could regulate the biosynthesis of GSH during the process of ferroptosis and serve as a target of p53 gene [27]. It's been confirmed that GLS2 has complex connections with cancers, and the up- or down-regulated expression level is significantly associated with patients' survival in different cancers [28–30]. Hence, it's easy to understand that the roles of GLS2 are likely to be tumor type-specific, and also enhance the notions that the implication of GLS2 in ferroptosis needs to be carefully interpreted in a context-dependent manner. These studies are in line with our results, pointing out GLS2 has positive correlation with patients' prognosis. It's reasonable to hypothesize the abnormal of GLS2 could promote the development of tumor through regulating the ferroptotic pathway. Although the mechanisms by which the GLS2 mediate the ferroptosis and leads to cancer remain elusive,

Niu Y et al gave us a hint that the occurrence of cancer may be a consequence of ferroptosis mediated by the miRNA/GLS2 axis [31].

Glutathione (GSH) is the most abundant antioxidant in the cell, which synthetizes from glutamate, cysteine and glycine [14, 32]. GCLM, also known as glutamate-cysteine ligase modifier, is the first-rate limiting enzyme of GSH synthesis. The inhibition of GCLM will induce the ferroptosis. The gene expression profiles show the GCLM level is up-regulated in many tumors [33–34]. Moreover, the GCLM expression level is negatively associated with patients' relapse free survival (RFS) and OS [33]. Our analysis is consistent with these findings, suggesting the GCLM is an oncogene (HR>1) in EAC. The existence of GLCM that drives ferroptosis has important implications for cancer therapy. A recent study by Sharma P identified the Andrographis, a medicine herb, could overcome the colorectal cancer chemoresistance by regulating the ferroptosis genes, such as GCLM [34]. Therefore, drugs that target ferroptosis can be exploited and provide an efficient strategy for clinical application. CARS1 alias: CARS (cysteinyl-tRNA synthetase), is still at infancy in the area of ferroptosis.

Study has shown that knockdown of CARS1 could cause increased transsulfuration pathway activity, and resistance to ferroptosis [14–15]. EMC2, also refer to TTC35, is ER (endoplasmic reticulum) membrane protein complex subunit 2. This gene share similarities with other ferroptosis-related gene, and its knockdown suppresses erastin-induced ferroptosis [14].

The notion that immunity promotes or suppresses the tumor is well accepted, and one of the most impactful anti-cancer therapies developed in recent years is the immune checkpoint therapy. Our results demonstrated that the immune statue was significantly different between the low-risk and high-risk EAC patients, including the DCs, CD8 + T cells, type I IFN response, type II IFN response et.al. The enigmatic and sophisticated relations linking immunity with ferroptosis are being gradually revealed with the progress of the experimental trials in vivo and vitro. Researchers found DCs in tumor-bearing hosts accumulate plenty of lipids and PUFAs, causing the impaired ability to present the antigen and stimulate the inadequate CD8 + T cells responses, lending support to the idea that DCs and CD8 + T cells contribute to the ferroptosis through regulating the lipids and PUFAs [35–36]. As expected, experiment ex vivo demonstrated that T cell lipid peroxidation could induce ferroptosis and prevent immunity to infection in the study by Matsushita M et al [37]. Consistent with the results of Matsushita M et al, preclinical models have confirmed CD8 + T cells could enhance ferroptosis-specific lipid peroxidation and increase ferroptosis by releasing the IFN-γ (II IFN), thus increasing the efficacy of immunotherapy [12]. In this study, we found the contents of DCs and CD8 + T cells were significantly higher in the low-risk group than those in high-risk group. One plausible explanation is DCs and CD8 + T cells activate the ferroptosis process by releasing signals, such as IFN-γ. Additionally, we also found the type I IFN (IFN-α, β) was also higher in the low-risk group, indicating the type I IFN may be necessary to initiate the ferroptosis. Undeniably, more work is warranted to confirm the above results.

The strength of this study is that we performed a systematically analysis based on the national database for the first time, and summarized the current knowledge about the ferroptosis genes in the EAC. Notably, it should be aware that the methods provided in this study did not meet all the requirements for the gene expression levels. Meanwhile, there are some limitations in our study. Firstly, the clinical information downloaded from the TCGA is incomplete, especially the therapy, which may be helpful to understand whether FRG are biomarkers of treatment. Secondly, the mechanism how ferroptosis modulate the precise process of EAC are unclear. Lastly, the prognostic model needs to be verified in a large-scale and multicenter clinical cohort. Notwithstanding its limitations, this study does provide a comprehensive overview of FRG profiles in EAC and these limitations can be solved if there are enough data in the future.

Conclusions

In conclusion, we identified differently expressed ferroptosis-related genes that may involve in the process in EAC. These genes have significant values in predicting the patients' OS and utilizing ferroptosis may be the therapeutic targets. Further studies are necessary to verify these results in our study.

Abbreviations

EAC: esophageal adenocarcinoma; ROS:reactive oxygen species; GSH:glutathione; FRG:ferroptosis-related genes; TCGA:The Cancer Genome Atlas; SDG:significantly different genes; FDR:false discovery rate; OS:overall survival; GO:Gene Ontology; KEGG:Kyoto Encyclopedia of Genes and Genomes; ROC:Receiver Operating Characteristic; AUC:area under curve; ssGSEA:single-sample gene set enrichment analysis; cDNA:complementary DNA; gDNA:genomic DNA; PCR:polymerase chain reaction; GAPDH:glyceraldehyde-3-phosphate dehydrogenase; HR:hazard ratio; PUFAs:polyunsaturated fatty acids; LOX:lipoxygenase; GLS2:glutaminase. RFS:relapse free survival.

Declarations

Ethics approval and consent to participate

This study was approved by the Internal Review Board of Shanghai East Hospital, Tongji University School of Medicine.

Consent for publication

Not applicable.

Availability of data and materials

All data were available in TCGA database (https://portal.gdc.cancer.gov). All the experimental data analyzed and displayed in the present manuscript are available from the corresponding author upon reasonable request.

The authors declare that they have no competing interests.

Funding

This study was supported by National Natural Science Foundation of China (NSFC, No. 81773266) to QC Li. The sponsor reviewed and approved the study conception. This work was also funded by Key Discipline Group Construction Project of Pudong Health Bureau of Shanghai China (No. PWZxq2017-13) to QC Li and Shanghai Municipal Health Commission, China (No. 20194Y0333) to L Dong. The sponsors participated in the design of the study and sponsored data collection, analysis, and writing of the manuscript.

Authors' contributions

LZ contributed to conception, design, data acquisition of the work. FGY contributed to interpretation and data analysis. LWW contributed to clinical specimen's acquisition and data collection. LD, ZYH and GXW performed RNA extraction and interpreted of PCR results. GHC conceived and designed the experimental protocol. QCL reviewed and approved the final version of the manuscript. All authors read and approved the final manuscript.

Acknowledgements

We would like to thank all the authors listed for their contribution to the present study.

References

1. Bray F, Ferlay J, Soerjomataram I, et al. Global cancer statistics 2018: GLOBOCAN estimates of incidence and mortality worldwide for 36 cancers in 185 countries. CA Cancer J Clin. 2018 Nov;68(6):394–424. doi:10.3322/caac.21492.
2. McColl KEL. What is causing the rising incidence of esophageal adenocarcinoma in the West and will it also happen in the East? J Gastroenterol. 2019 Aug;54(8):669–73. doi:10.1007/s00535-019-01593-7.
3. Alsop BR, Sharma P. Esophageal Cancer. Gastroenterol Clin North Am. 2016 Sep;45(3):399–412. doi:10.1016/j.gtc.2016.04.001.
4. Coleman HG, Xie SH, Lagergren J. The Epidemiology of Esophageal Adenocarcinoma. Gastroenterology. 2018 Jan;154(2):390–405. doi:10.1053/j.gastro.2017.07.046.
5. Xu T, Ding W, Ji X, et al. Molecular mechanisms of ferroptosis and its role in cancer therapy. J Cell Mol Med. 2019 Aug;23(8):4900–12. doi:10.1111/jcmm.14511. Epub 2019 Jun 24.
6. Shen Z, Song J, Yung BC, et al. Emerging Strategies of Cancer Therapy Based on Ferroptosis. Adv Mater. 2018 Mar;30(12):e1704007. doi:10.1002/adma.201704007.
7. Dixon SJ, Lemberg KM, Lamprecht MR, et al. Ferroptosis: an iron-dependent form of nonapoptotic cell death. Cell. 2012 May 25;149(5):1060-72. doi: 10.1016/j.cell.2012.03.042.

8. Yang WS, SriRamaratnam R, Welsch ME, et al. Regulation of ferroptotic cancer cell death by GPX4. Cell. 2014 Jan 16;156(1–2):317–331. doi: 10.1016/j.cell.2013.12.010.
9. Eling N, Reuter L, Hazin J, et al. Identification of artesunate as a specific activator of ferroptosis in pancreatic cancer cells. Oncoscience. 2015 May 2;2(5):517 – 32. doi: 10.18632/oncoscience.160.
10. Basuli D, Tesfay L, Deng Z, et al. Iron addiction: a novel therapeutic target in ovarian cancer. Oncogene. 2017 Jul 20;36(29):4089–4099. doi: 10.1038/onc.2017.11.
11. Wang D, Xie N, Gao W, et al. The ferroptosis inducer erastin promotes proliferation and differentiation in human peripheral blood mononuclear cells. Biochem Biophys Res Commun. 2018 Sep 10;503(3):1689–1695. doi: 10.1016/j.bbrc.2018.07.100.
12. Wang W, Green M, Choi JE, et al. CD8 + T cells regulate tumour ferroptosis during cancer immunotherapy. Nature. 2019 May;569(7755):270–4. doi:10.1038/s41586-019-1170-y.
13. Stockwell BR, Jiang X. A Physiological Function for Ferroptosis in Tumor Suppression by the Immune System. Cell Metab. 2019 Jul 2;30(1):14–15. doi: 10.1016/j.cmet.2019.06.012.
14. Stockwell BR, Friedmann Angeli JP, Bayir H, et al. Ferroptosis: A Regulated Cell Death Nexus Linking Metabolism, Redox Biology, and Disease. Cell. 2017 Oct 5;171(2):273–285. doi: 10.1016/j.cell.2017.09.021.
15. Hassannia B, Vandenabeele P, Vanden Berghe T. Targeting Ferroptosis to Iron Out Cancer. Cancer Cell. 2019 Jun 10;35(6):830–849. doi: 10.1016/j.ccell.2019.04.002.
16. Bersuker K, Hendricks JM, Li Z, et al. The CoQ oxidoreductase FSP1 acts parallel to GPX4 to inhibit ferroptosis. Nature. 2019 Nov;575(7784):688–92. doi:10.1038/s41586-019-1705-2.
17. Doll S, Freitas FP, Shah R, et al. FSP1 is a glutathione-independent ferroptosis suppressor. Nature. 2019 Nov;575(7784):693–8. doi:10.1038/s41586-019-1707-0.
18. Rooney MS, Shukla SA, Wu CJ, et al. Molecular and genetic properties of tumors associated with local immune cytolytic activity. Cell. 2015 Jan 15;160(1–2):48–61. doi: 10.1016/j.cell.2014.12.033.
19. Yuan H, Li X, Zhang X, et al. Identification of ACSL4 as a biomarker and contributor of ferroptosis. Biochem Biophys Res Commun. 2016 Sep 23;478(3):1338-43. doi: 10.1016/j.bbrc.2016.08.124.
20. Wang SJ, Li D, Ou Y, et al. Acetylation Is Crucial for p53-Mediated Ferroptosis and Tumor Suppression. Cell Rep. 2016 Oct 4;17(2):366–373. doi: 10.1016/j.celrep.2016.09.022.
21. Zhang Y, Shi J, Liu X, et al. BAP1 links metabolic regulation of ferroptosis to tumour suppression. Nat Cell Biol. 2018 Oct;20(10):1181–92. doi:10.1038/s41556-018-0178-0.
22. Reis A, Spickett CM. Chemistry of phospholipid oxidation. Biochim Biophys Acta. 2012 Oct;1818(10):2374–87. doi:10.1016/j.
23. Gaschler MM, Stockwell BR. Lipid peroxidation in cell death. Biochem Biophys Res Commun. 2017 Jan 15;482(3):419–425. doi: 10.1016/j.bbrc.2016.10.086.
24. Lu SC. Regulation of glutathione synthesis. Mol Aspects Med. 2009 Feb-Apr;30(1–2):42–59. doi: 10.1016/j.mam.2008.05.005.

25. Yant LJ, Ran Q, Rao L, et al. The selenoprotein GPX4 is essential for mouse development and protects from radiation and oxidative damage insults. Free Radic Biol Med. 2003 Feb;15(4):496–502. doi:10.1016/s0891-5849(02)01360-6. 34) .
26. Matés JM, Segura JA, Martín-Rufián M, et al. Glutaminase isoenzymes as key regulators in metabolic and oxidative stress against cancer. Curr Mol Med. 2013 May;13(4):514–34. doi:10.2174/1566524011313040005.
27. Suzuki S, Tanaka T, Poyurovsky MV, et al. Phosphate-activated glutaminase (GLS2), a p53-inducible regulator of glutamine metabolism and reactive oxygen species. Proc Natl Acad Sci U S A. 2010 Apr 20;107(16):7461-6. doi: 10.1073/pnas.1002459107.
28. Li HJ, Li X, Pang H, et al. Long non-coding RNA UCA1 promotes glutamine metabolism by targeting miR-16 in human bladder cancer. Jpn J Clin Oncol. 2015 Nov;45(11):1055–63. doi:10.1093/jjco/hyv132.
29. Katt WP, Lukey MJ, Cerione RA. A tale of two glutaminases: homologous enzymes with distinct roles in tumorigenesis. Future Med Chem. 2017 Jan;9(2):223–43. doi:10.4155/fmc-2016-0190.
30. Zhang J, Wang C, Chen M, et al. Epigenetic silencing of glutaminase 2 in human liver and colon cancers. BMC Cancer. 2013 Dec;14:13:601. doi:10.1186/1471-2407-13-601.
31. Niu Y, Zhang J, Tong Y, et al. Physcion 8-O-β-glucopyranoside induced ferroptosis via regulating miR-103a-3p/GLS2 axis in gastric cancer. Life Sci. 2019 Nov 15;237:116893. doi: 10.1016/j.lfs.2019.116893.
32. Meister A. Selective modification of glutathione metabolism. Science. 1983 Apr 29;220(4596):472-7. doi: 10.1126/science.6836290.
33. Harris IS, Treloar AE, Inoue S, et al. Glutathione and thioredoxin antioxidant pathways synergize to drive cancer initiation and progression. Cancer Cell. 2015 Feb 9;27(2):211 – 22. doi: 10.1016/j.ccell.2014.11.019.
34. Sharma P, Shimura T, Banwait JK, et al. Andrographis-mediated chemosensitization through activation of ferroptosis and suppression of β-catenin/Wnt-signaling pathways in colorectal cancer. Carcinogenesis. 2020 Aug 24:bgaa090. doi: 10.1093/carcin/bgaa090.
35. Veglia F, Tyurin VA, Mohammadyani D, et al. Lipid bodies containing oxidatively truncated lipids block antigen cross-presentation by dendritic cells in cancer. Nat Commun. 2017 Dec 14;8(1):2122. doi: 10.1038/s41467-017-02186-9.
36. Ramakrishnan R, Tyurin VA, Veglia F, et al. Oxidized lipids block antigen cross-presentation by dendritic cells in cancer. J Immunol. 2014 Mar 15;192(6):2920–31. doi: 10.4049/jimmunol.1302801.
37. Matsushita M, Freigang S, Schneider C, et al. T cell lipid peroxidation induces ferroptosis and prevents immunity to infection. J Exp Med. 2015 Apr 6;212(4):555 – 68. doi: 10.1084/jem.20140857.

Tables

Table 1 significantly different FRG expression levels in EAC and normal tissue

gene	normal	EAC	logFC	P value
ACSL4	11.274	18.158	0.688	0.02
AIFM2	3.554	5.584	0.652	0.022
AKR1C1	6.188	3.015	-1.037	0.006
AKR1C2	6.788	3.245	-1.065	0.019
ALOX5	2.671	8.927	1.741	0.021
CARS1	4.068	5.739	0.496	0.006
DPP4	6.142	12.714	1.05	0.005
EMC2	5.861	8.602	0.553	0.001
FANCD2	1.29	3.465	1.426	0.001
FDFT1	28.431	47.563	0.742	0.025
G6PD	14.208	27.87	0.972	0.006
GCLM	4.08	7.077	0.795	0.001
GSS	16.051	28.628	0.835	0
HSBP1	6.611	9.82	0.571	0.001
HSPB1	324.993	369.728	0.186	0.011
MT1G	336.078	54.328	-2.629	0
NFE2L2	45.899	28.153	-0.705	0
NFS1	3.264	5.003	0.616	0.01
NOX1	0.2	5.601	4.809	0
PHKG2	2.393	4.149 0.794	0	0.003
PTGS2	2.205	8.034	1.865	0.002
RPL8	259.463	445.943	0.781	0.001
SAT1	94.001	155.854	0.729	0.016
SLC1A5	22.655	55.248	1.286	0
SLC7A11	2.194	5.322	1.279	0.01
SQLE	8.165	18.257	1.161	0.001
TFRC	12.433	40.774	1.713	0
TP53	9.948	19.273	0.954	0.02

LogFC: log fold change; FDR: false discovery rate

Figures

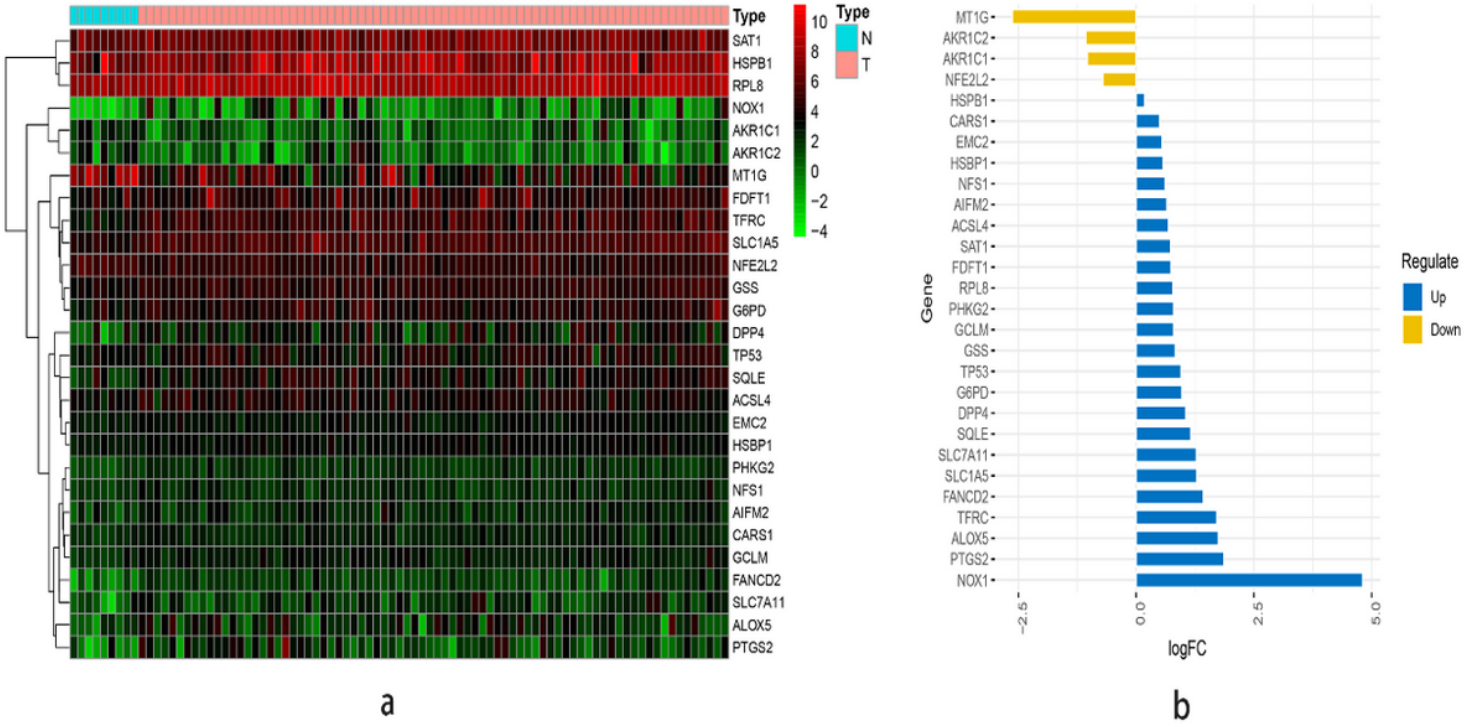

Figure 1

Identification of SDG in normal and EAC tissues. (a) heatmap of SDG. Green represented down-regulation and red represented up-regulation of genes. (b) deviation plot of SDG. Yellow bars represented 4 down-regulated genes; blue bars represented 24 up-regulated genes. N: normal, T: tumor (EAC).

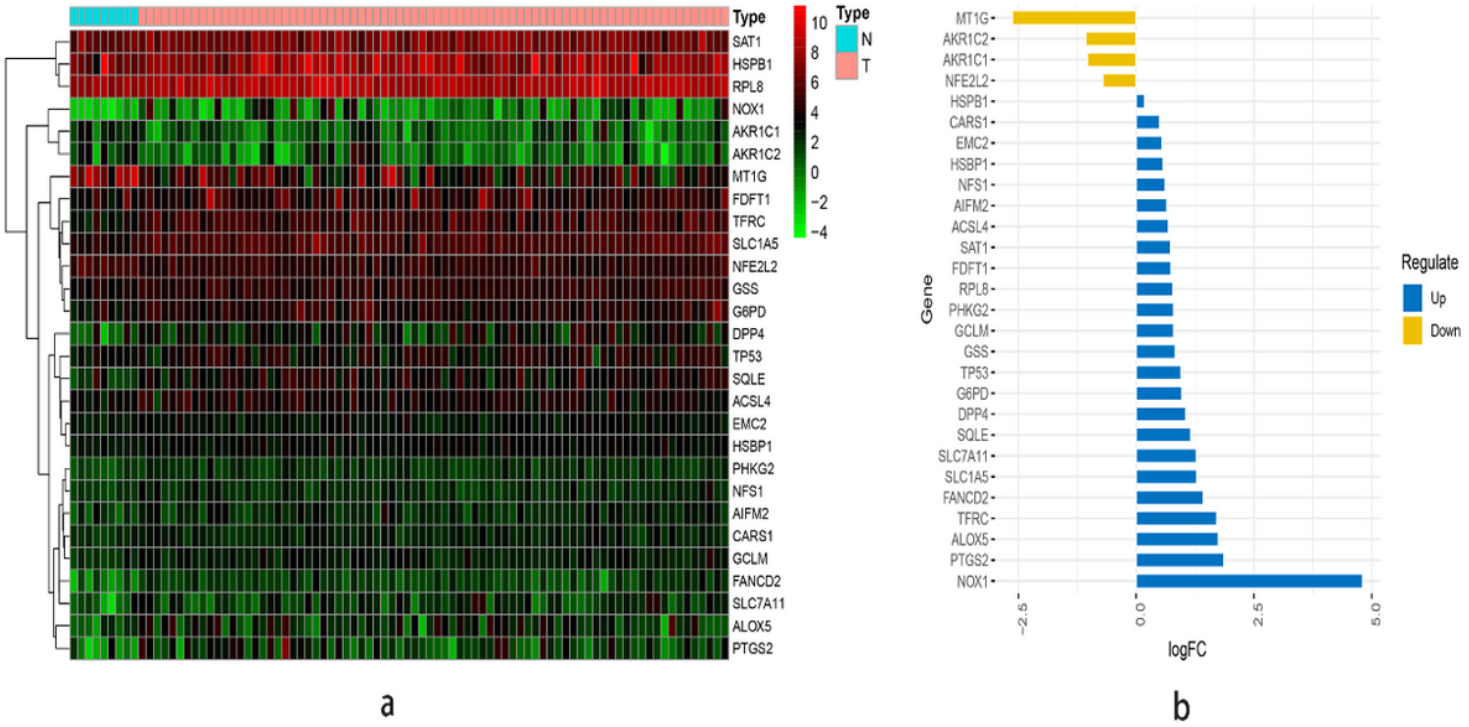

Figure 1

Identification of SDG in normal and EAC tissues. (a) heatmap of SDG. Green represented down-regulation and red represented up-regulation of genes. (b) deviation plot of SDG. Yellow bars represented 4 down-regulated genes; blue bars represented 24 up-regulated genes. N: normal, T: tumor (EAC).

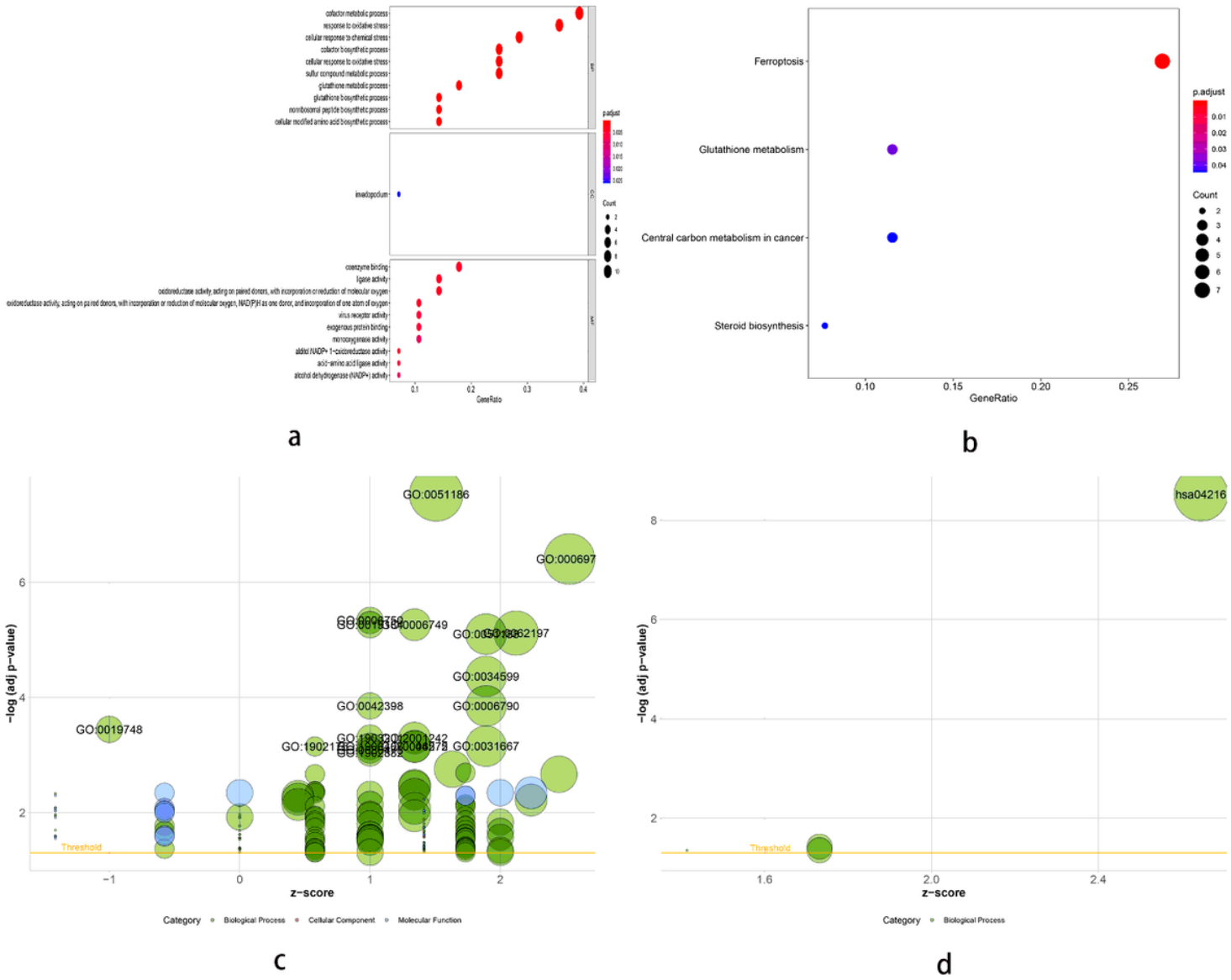

Figure 2

Representative results of GO (a, c) and KEGG (b, d). bubble plot of GO (a) and KEGG (b) analyses. Results of GO (c) and KEGG (d) in the form of gene ID. The larger bubble indicates the more obvious enrichment.

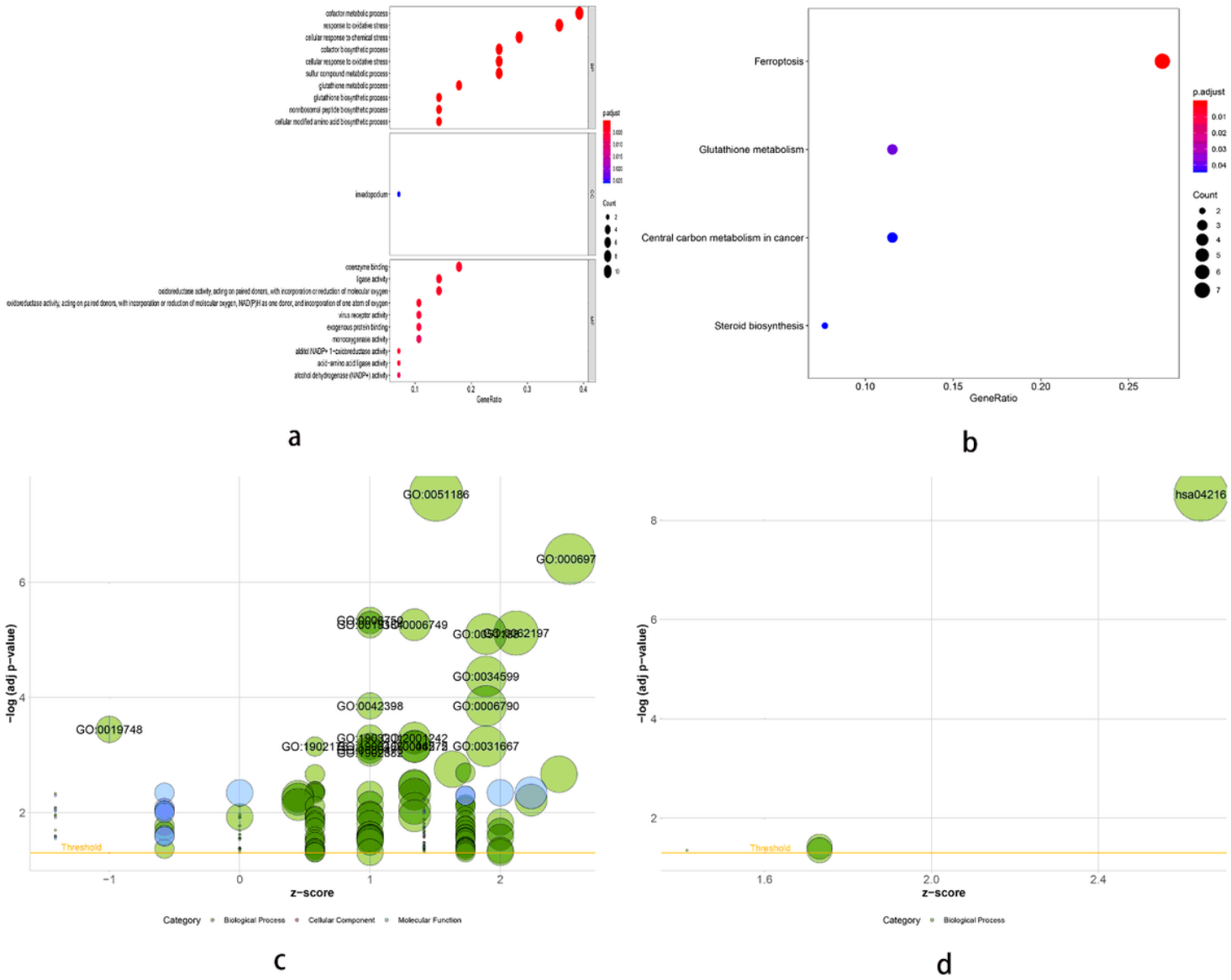

Figure 2

Representative results of GO (a, c) and KEGG (b, d). bubble plot of GO (a) and KEGG (b) analyses. Results of GO (c) and KEGG (d) in the form of gene ID. The larger bubble indicates the more obvious enrichment.

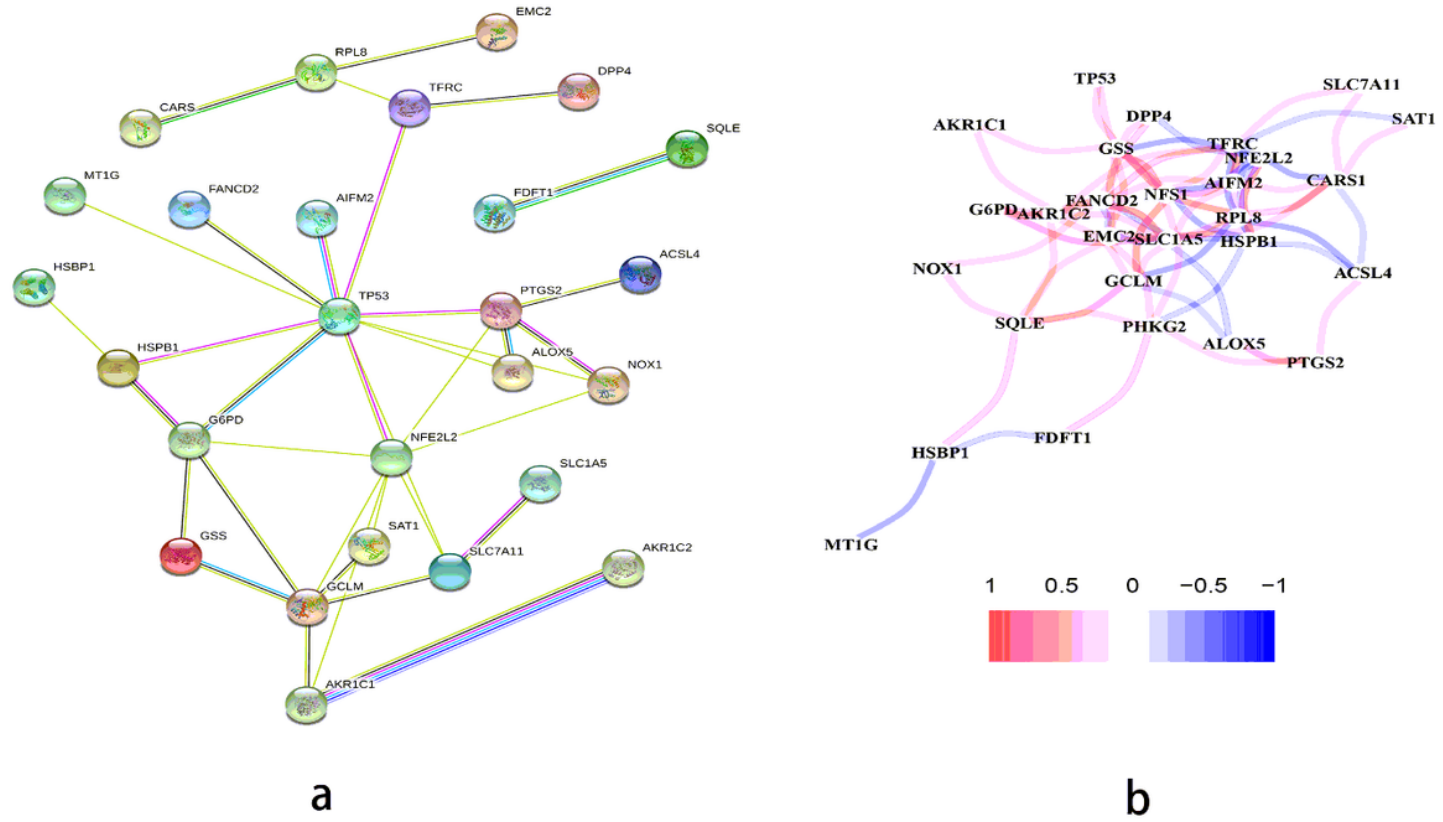

Figure 3

Gene interactions and correlations plots of SDG. (a)The gene network downloaded from the STRING database indicated the interactions among the SDG. (b)The correlation network of genes. Red line represents the positive correlation, while the blue line represents the negative correlation.

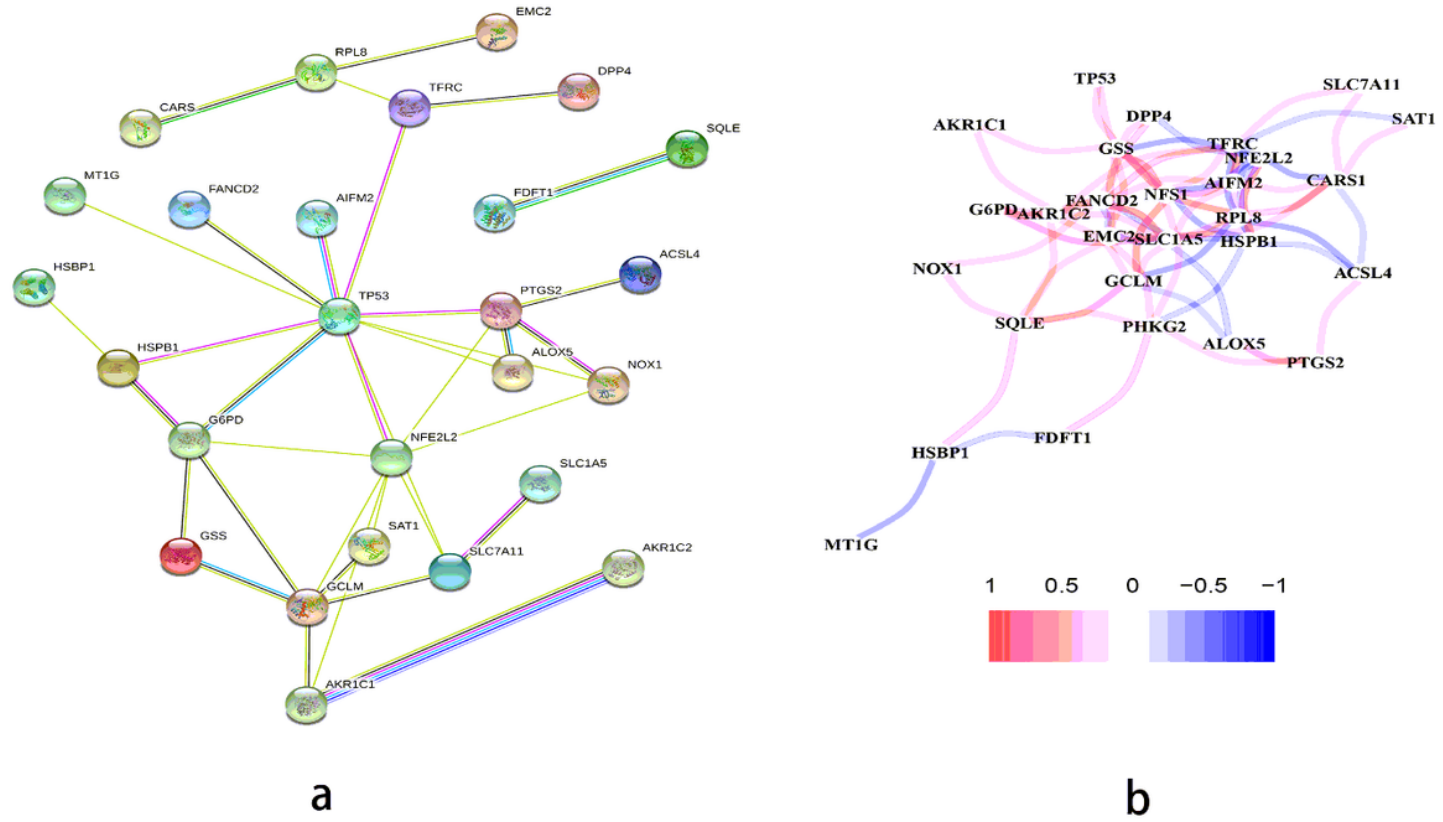

Figure 3

Gene interactions and correlations plots of SDG. (a)The gene network downloaded from the STRING database indicated the interactions among the SDG. (b)The correlation network of genes. Red line represents the positive correlation, while the blue line represents the negative correlation.

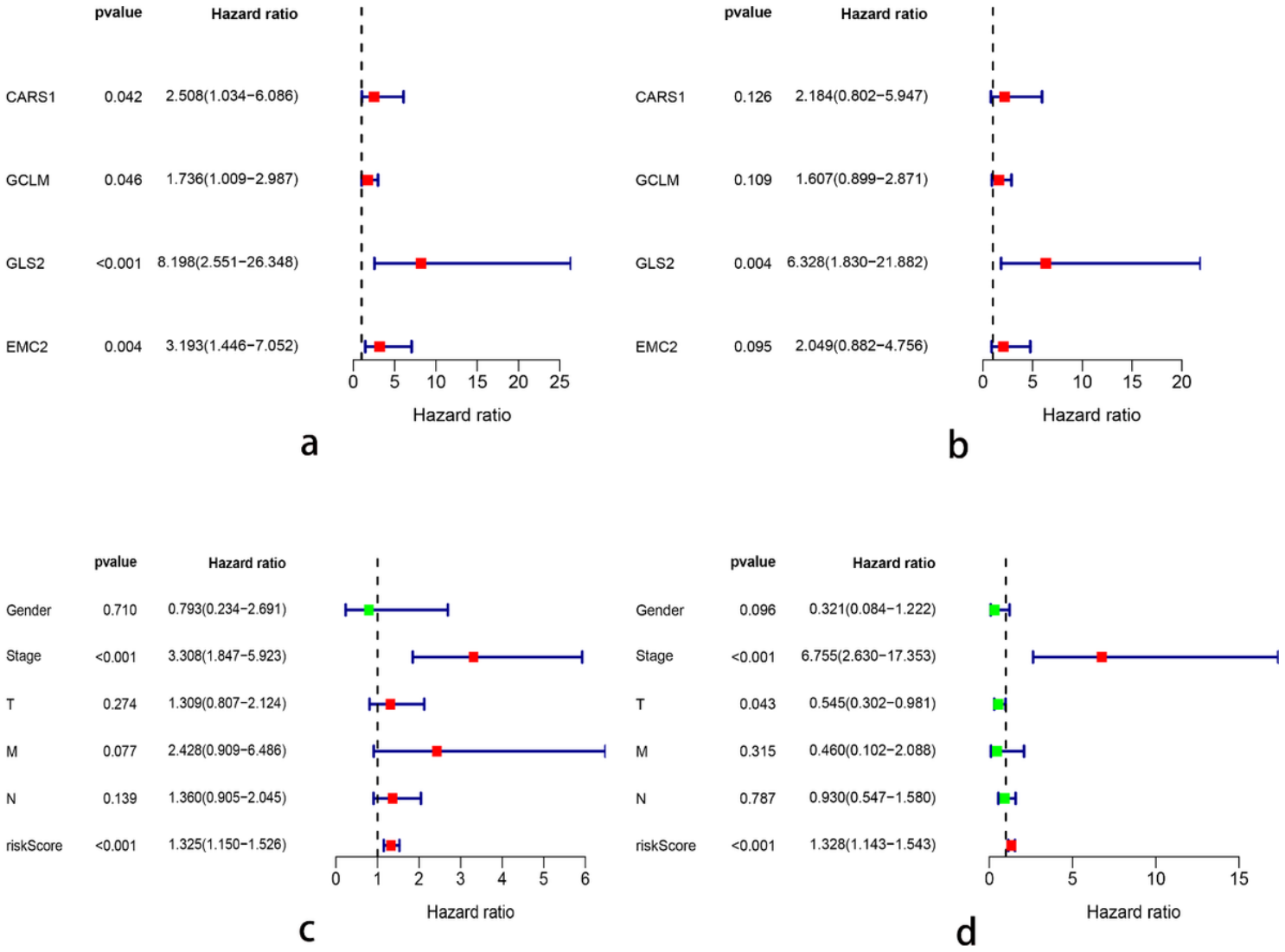

Figure 4

Results of the univariate and multivariate cox analysis of the OS in EAC patients. FRG prognostic values in the univariate (a) and multivariate cox analysis (b). Risk factors analysis of OS in the univariate (c) and multivariate cox regression (d). HR: hazard ratio.

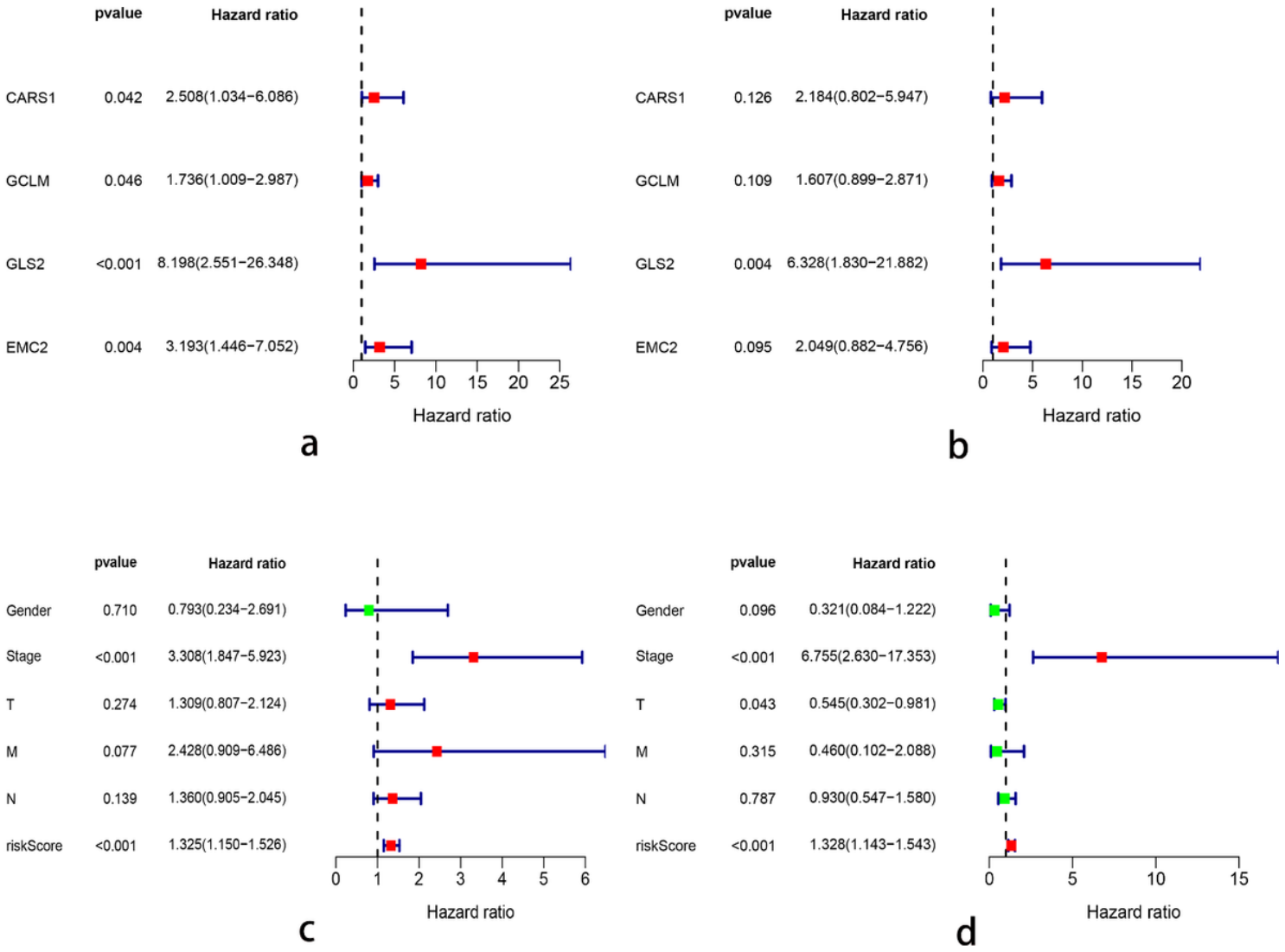

Figure 4

Results of the univariate and multivariate cox analysis of the OS in EAC patients. FRG prognostic values in the univariate (a) and multivariate cox analysis (b). Risk factors analysis of OS in the univariate (c) and multivariate cox regression (d). HR: hazard ratio.

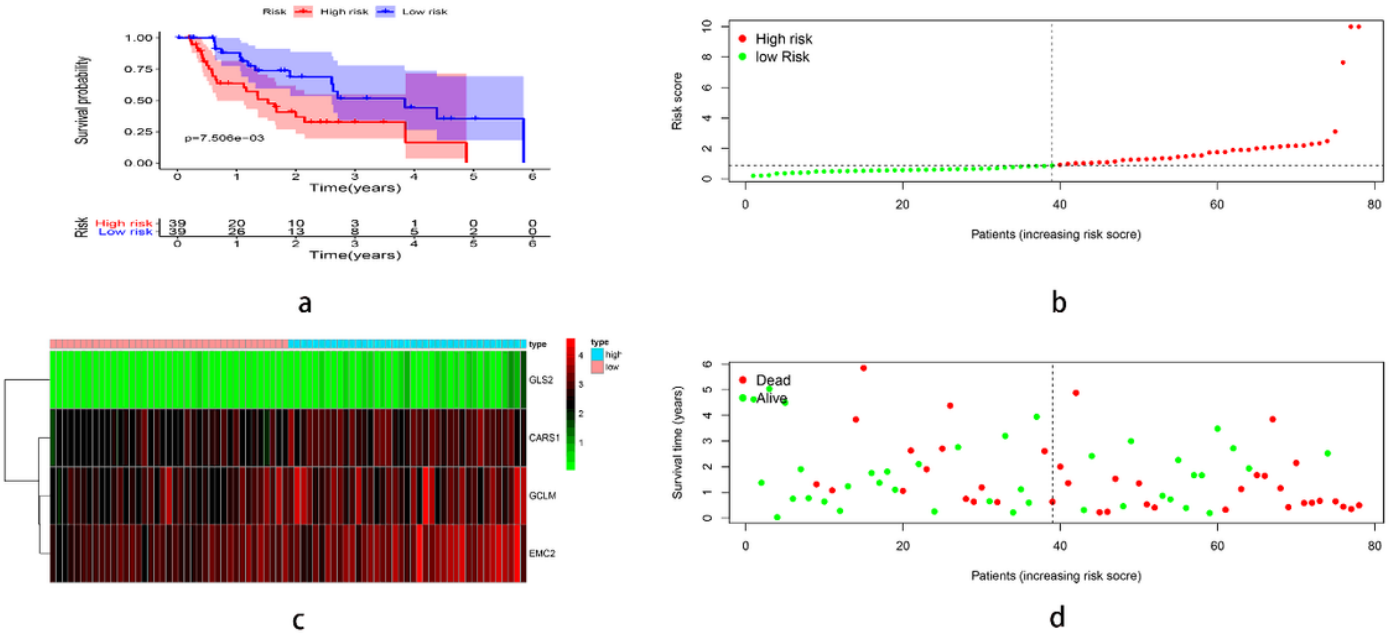

Figure 5

Kaplan-Meier curve and prognostic hazard curves. Kaplan-Meier survival curve (a). Risk score curve plot (b). The dotted line indicated the individual inflection point of the risk score curve, by which the patients were categorized into low-risk (green) and high-risk (red) groups. Risk score heatmap (c). The colors from green to red indicated the expression level from low to high. Risk score scatter plot of high-risk and low-risk (d). Red dots represented the dead patients and green represented the alive. With the increase of risk score, more patients died.

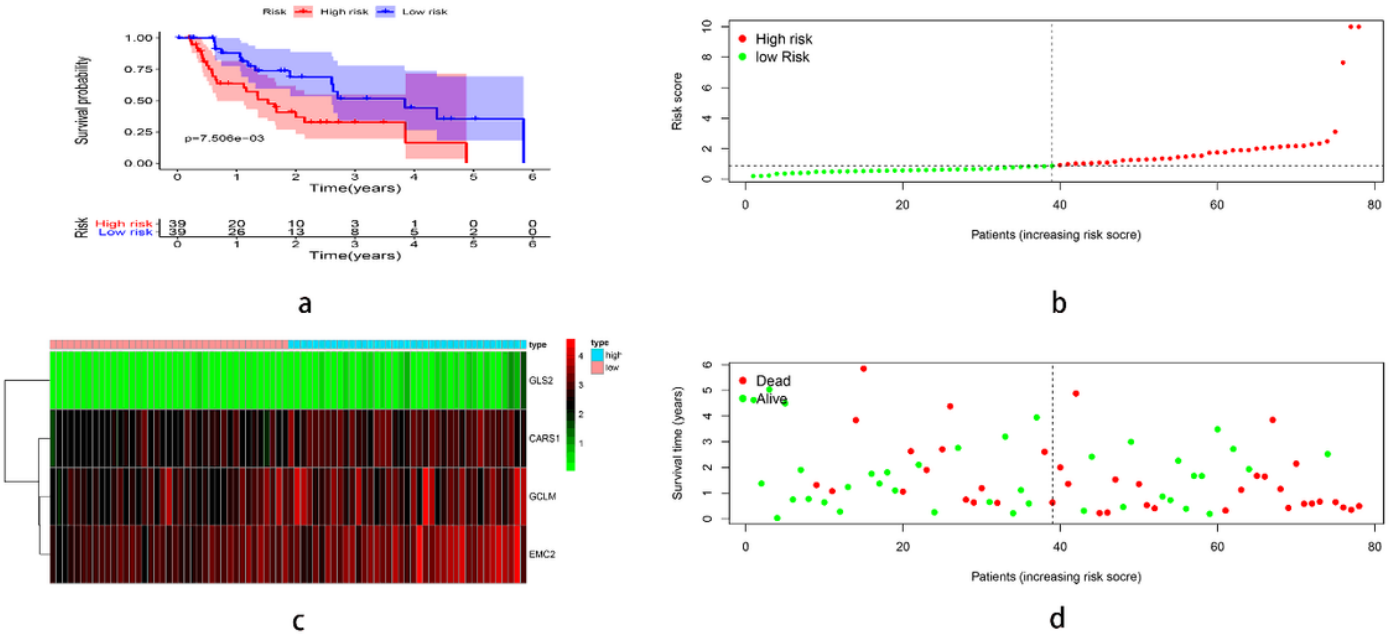

Figure 5

Kaplan-Meier curve and prognostic hazard curves. Kaplan-Meier survival curve (a). Risk score curve plot (b). The dotted line indicated the individual inflection point of the risk score curve, by which the patients were categorized into low-risk (green) and high-risk (red) groups. Risk score heatmap (c). The colors from green to red indicated the expression level from low to high. Risk score scatter plot of high-risk and low-risk (d). Red dots represented the dead patients and green represented the alive. With the increase of risk score, more patients died.

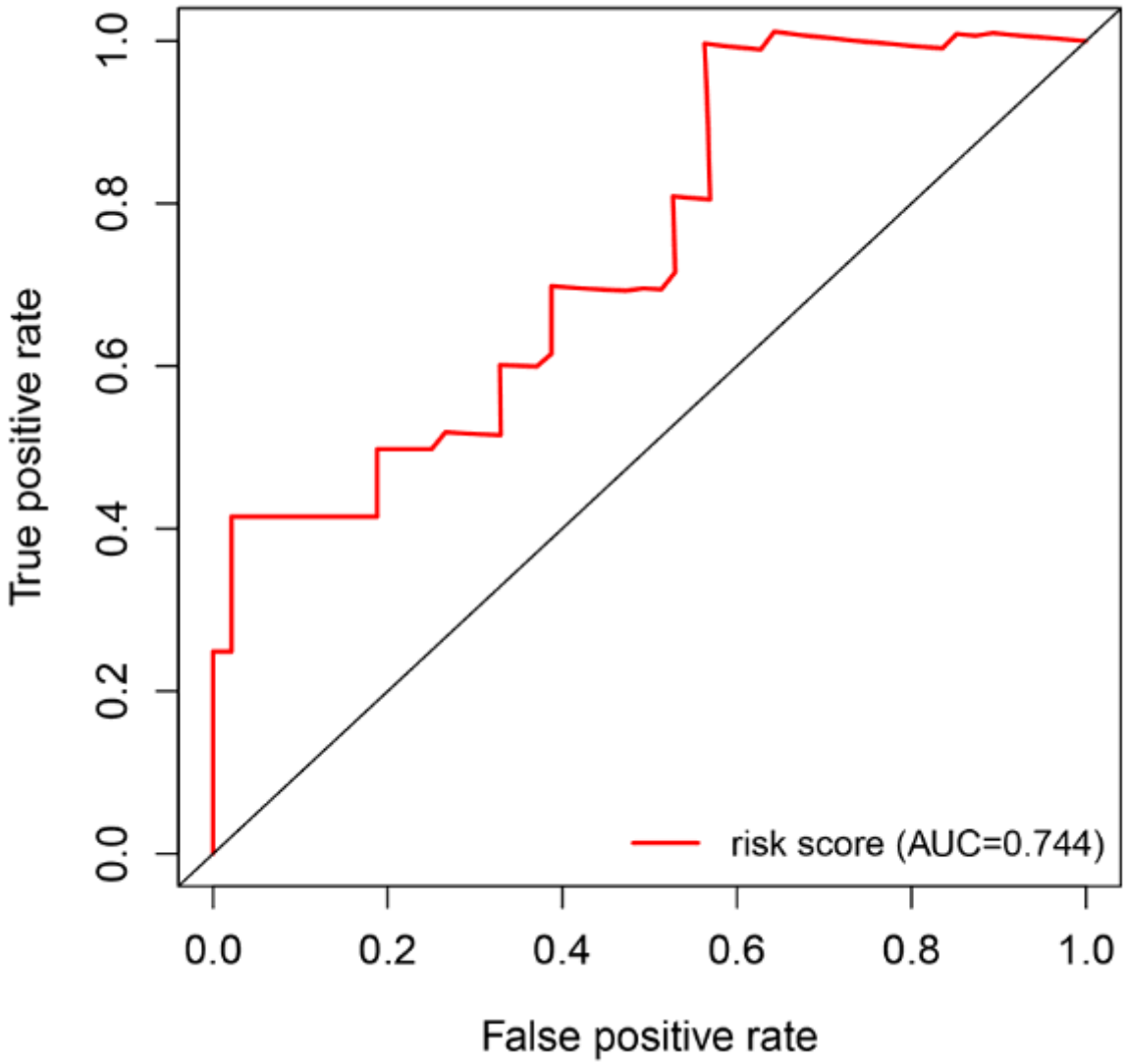

Figure 6

ROC curve of risk score. The AUC ranges from 0.5 to 1.0, with near 1.0 indicating perfect predictive ability.

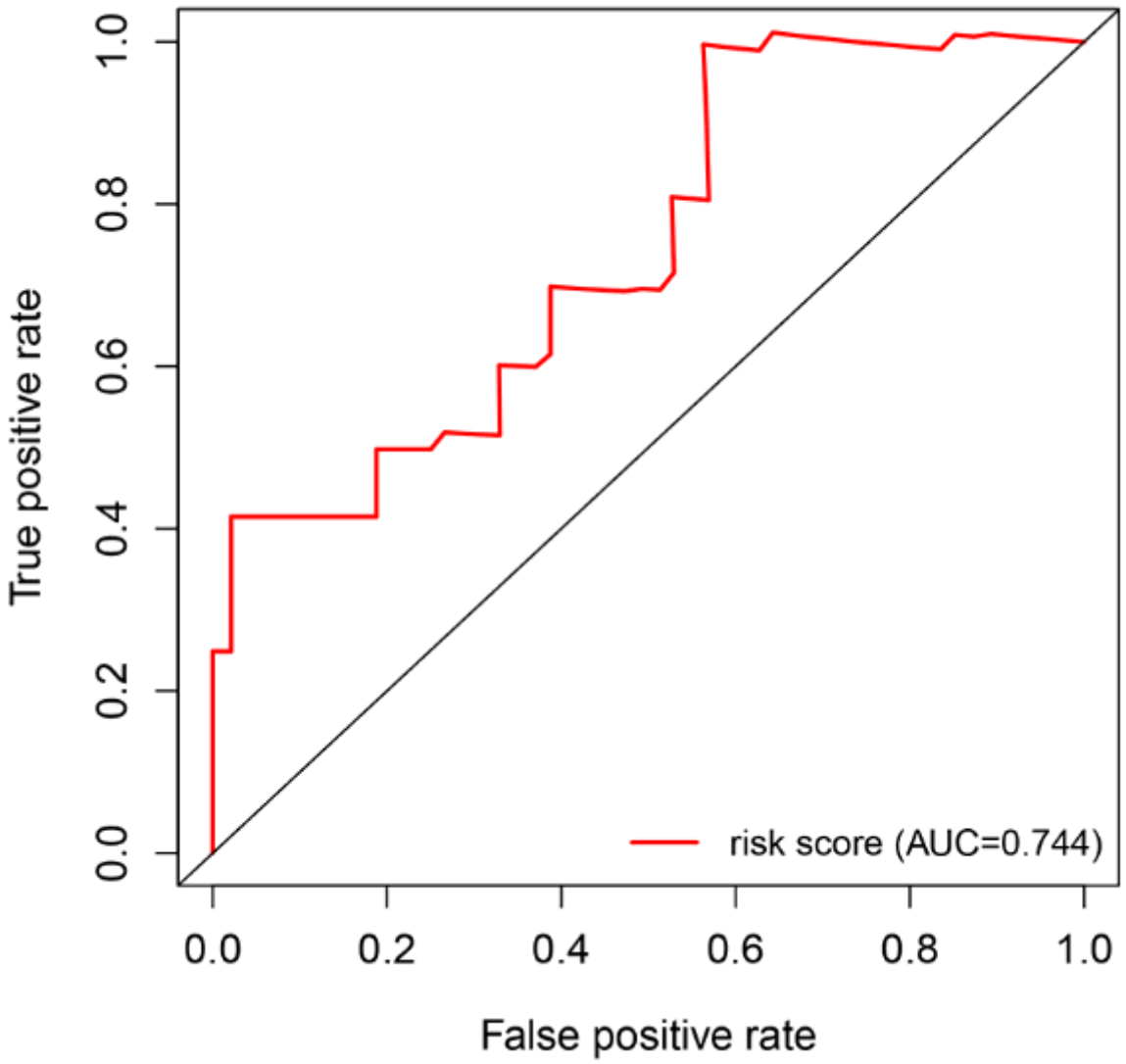

Figure 6

ROC curve of risk score. The AUC ranges from 0.5 to 1.0, with near 1.0 indicating perfect predictive ability.

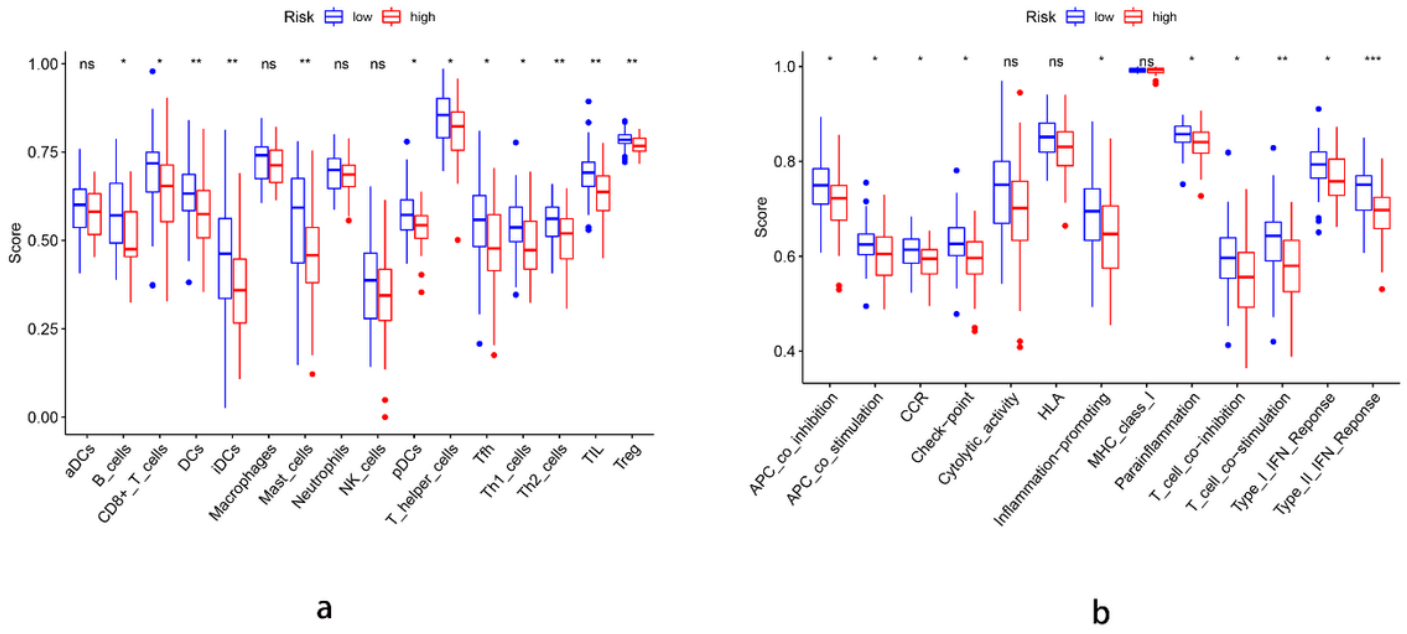

Figure 7

Comparison of the ssGSEA scores between the high-risk and low-risk groups. The scores of 16 immune cells (a) and 13 immune-related functions (b) are displayed in boxplots. DC: dendritic cell; TIL: tumor infiltrating lymphocyte; CCR: cytokine-cytokine receptor; APC: antigen presenting cells. Adjusted P values were showed as: ns, not significant; *, P< 0.05; **, P< 0.01; ***, P< 0.001.

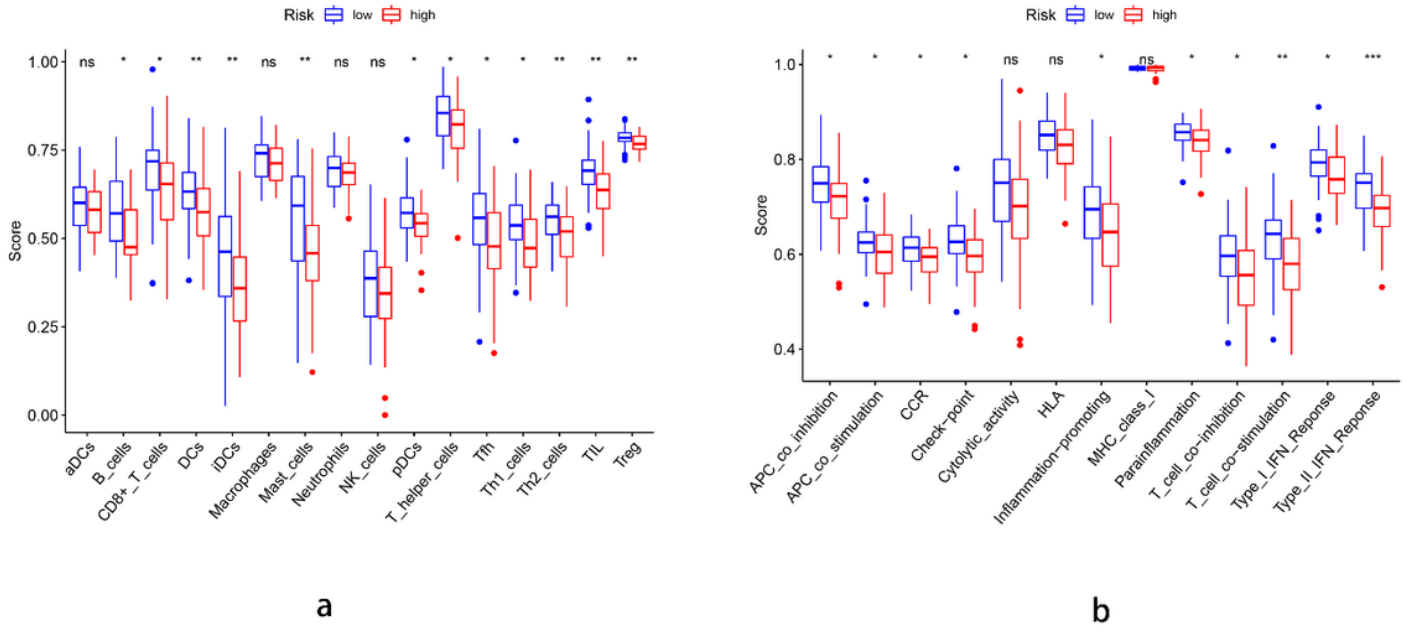

Figure 7

Comparison of the ssGSEA scores between the high-risk and low-risk groups. The scores of 16 immune cells (a) and 13 immune-related functions (b) are displayed in boxplots. DC: dendritic cell; TIL: tumor infiltrating lymphocyte; CCR: cytokine-cytokine receptor; APC: antigen presenting cells. Adjusted P values were showed as: ns, not significant; *, P< 0.05; **, P< 0.01; ***, P< 0.001.

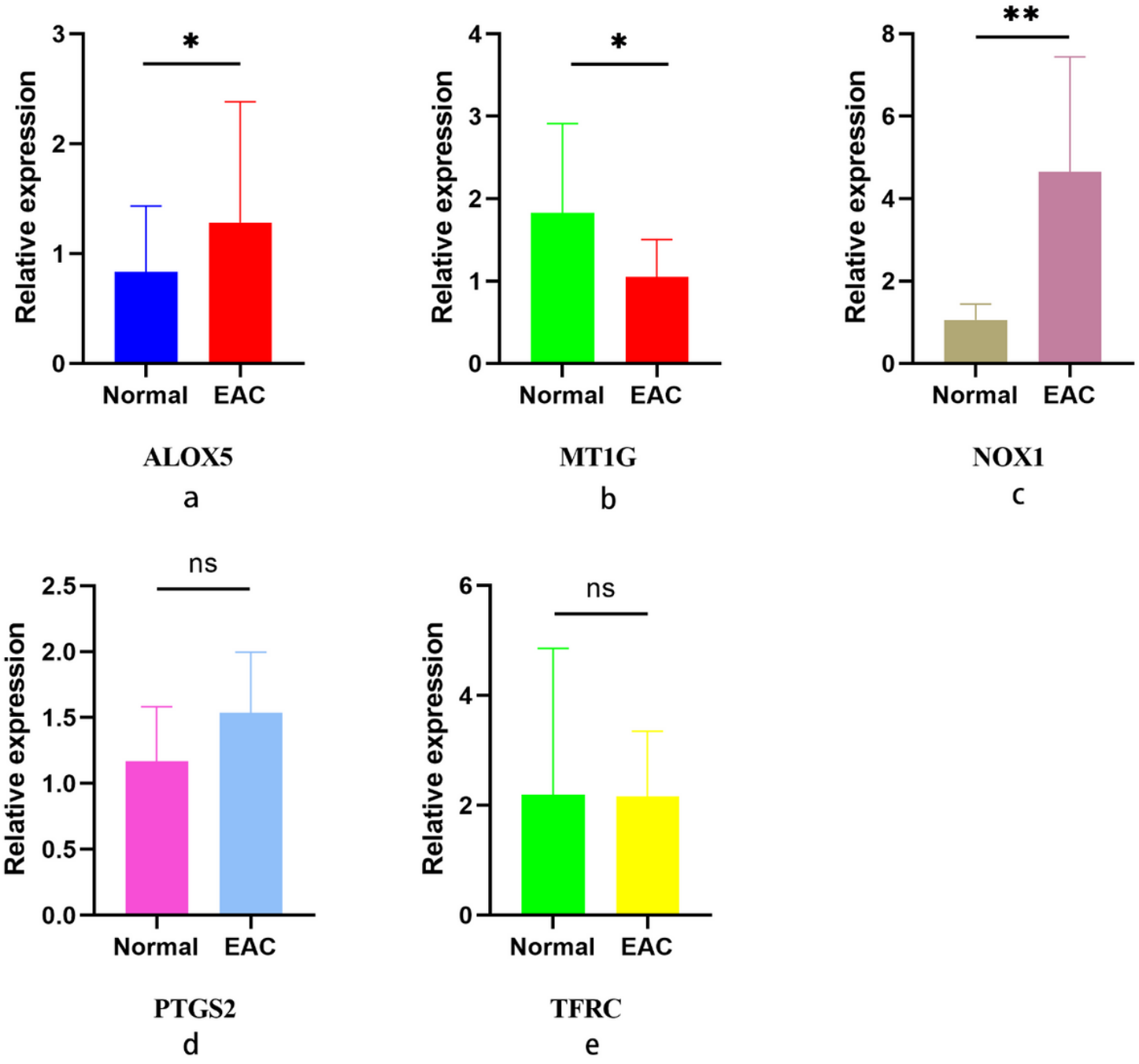

Figure 8

The relative expression levels of the five genes in normal and EAC tissues. The ALOX5 (a), NOX1 (c) were up-regulated significantly and MT1G (b) were down-regulated in the EAC tissues. No significant differences were observed in the PTGS2 (d) and TFRC (e). *: P< 0.05; **: P< 0.01, ns: not significant.

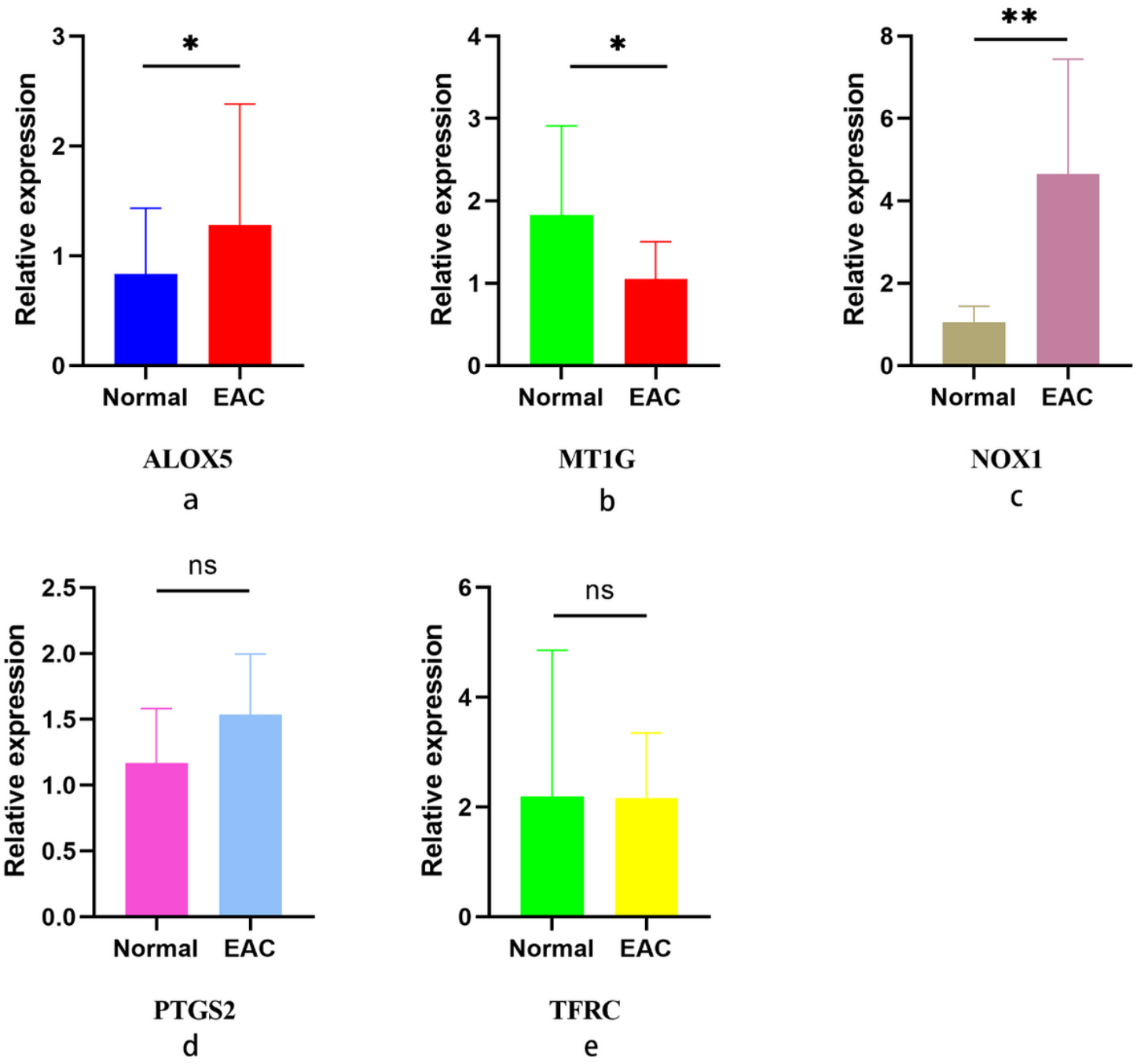

Figure 8

The relative expression levels of the five genes in normal and EAC tissues. The ALOX5 (a), NOX1 (c) were up-regulated significantly and MT1G (b) were down-regulated in the EAC tissues. No significant differences were observed in the PTGS2 (d) and TFRC (e). *: P< 0.05; **: P< 0.01, ns: not significant.

Supplementary Files

This is a list of supplementary files associated with this preprint. Click to download.

- SupplementaryTableS1.docx
- SupplementaryTableS2.xls
- SupplementaryTableS2.xls
- SupplementaryTableS3.docx
- SupplementaryTableS3.docx